Intelligent Control and Automation, 2026, 17(4), 299-317
https://www.scirp.org/journal/ica
ISSN Online: 2153-0661
ISSN Print: 2153-0653

An Enhanced CMD Technique for Bearing Health Condition Monitoring

Megha Malusare, Ran Zhao, Wilson Wang

Department of Mechatronics Engineering, Lakehead University, Barrie, Ontario, Canada
Email: wilson.wang@lakeheadu.ca

How to cite this paper: Malusare, M., Zhao, R. and Wang, W. (2026) An Enhanced CMD Technique for Bearing Health Condition Monitoring. *Intelligent Control and Automation*, **17**, 299-317.
https://doi.org/10.4236/ica.2026.174014

Received: November 5, 2026
Accepted: November 23, 2026
Published: November 26, 2026

Copyright © 2026 by author(s) and Scientific Research Publishing Inc.
This work is licensed under the Creative Commons Attribution International License (CC BY 4.0).
http://creativecommons.org/licenses/by/4.0/

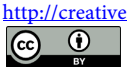

Open Access

Abstract

Rolling element bearings are widely used in rotating machines in various industries. Reliable and automatic bearing condition monitoring are critically needed in industries to improve machine operation efficiency and safety. The key to improving bearing condition monitoring reliability is to use inputs obtained from robust bearing fault detection techniques. Although many bearing fault detection techniques have been proposed in literature, reliable bearing fault diagnosis remains a challenging task in research, especially in automatic machine condition monitoring because bearing fault features are usually weak, nonlinear and modulated by other vibration signals. A new enhanced chirp mode decomposition (eCMD) technique is proposed in this work to improve reliability of bearing fault detection. The expected fault trajectories are used to provide clear physical justification for signal decomposition. An envelope demodulation approach is suggested to suppress noise and interference and highlight the second-order cyclic impact features for bearing fault detection and diagnosis. The effectiveness of the proposed eCMD technique is examined by experimental tests corresponding to different bearing conditions.

Keywords

Machine Condition Monitoring, Bearing Fault Detection, Adaptive Chirp Mode Decomposition, Envelope Demodulation, Signal Processing, Bearing Fault Diagnosis

1. Introduction

Rolling element bearings are commonly used in rotating machines in various industrial applications such as vehicles, motors, robots and turbines. It has been documented that more than 50% of abnormalities in rotating machines can be attributed to bearing defects [1] [2]. The health condition of bearings affects ma-

chine efficiency and safety, since their failures may result in machinery breakdown, less productive efficiency, unexpected costs in repairs or even catastrophic accidents [3] [4]. Therefore, reliable automatic bearing condition monitoring is critically needed in industries for more effective bearing fault detection to prevent unexpected failures and avoid costly downtime. The key to improving reliability of machine condition monitoring is to use robust input features that are sensitive to bearing faults and insensitive to noise and interference. Input fault features are obtained using appropriate signal processing techniques. Although many signal processing techniques have been proposed in literature for bearing fault detection, reliable bearing fault detection and fault type diagnosis remain a challenging task [5] [6]. It is because a bearing is not a mechanical component, like a gear or a shaft, but it is a system comprising a rotating ring (e.g., inner race), a fixed ring (e.g., outer race), rolling elements and a cage, as illustrated in **Figure 1**. Bearing signals are usually weak in magnitude, non-stationary, and modulated by other vibration signals. The bearing fault characteristic frequencies depend on the geometric parameters of the bearing [3]. When periodic impacts in the vibration match a characteristic frequency or its harmonic, resonance occurs. The resonance features will be used for bearing fault diagnosis [7] [8]. Therefore, the main challenge is how to extract representative features from the highly non-stationary and noise-contained vibration signals.

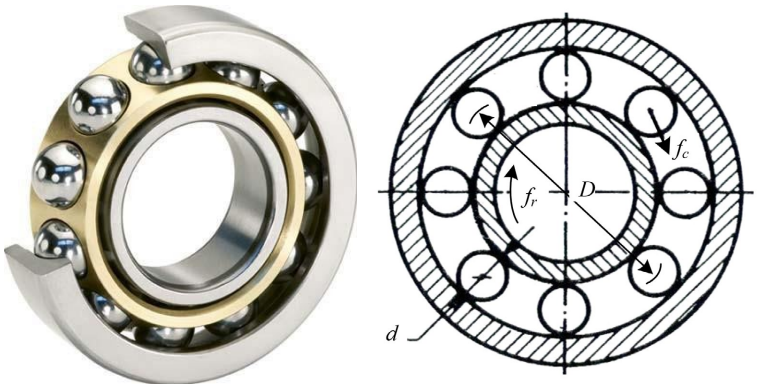

Figure 1. Structure of a rolling element (ball) bearing.

Fault feature extraction can be undertaken using appropriate signal processing techniques in the time-domain, frequency-domain, or time-frequency domain, respectively. Recent studies, however, focus on the time-frequency domain analysis, which could be more suitable for analysis of bearing fault-related nonstationary and transient features [1]. Traditional time-frequency methods, such as the short-time Fourier transform (FT) [9], continuous wavelet transform (CWT) [10] and Hilbert-Huang transform (HHT) [11], have been used in bearing fault diagnosis. However, the short-time FT suffers from limited simultaneous time-frequency localization due to its fixed window resolutions. The CWT is computationally expensive and sensitive to wavelet selection. Empirical mode decomposition (EMD) in the HHT is highly sensitive to mode mixture and end-effects, which

reduces the efficiency in extracting instantaneous frequencies. These limitations have motivated the development of advanced approaches in the time-frequency domain.

The combined multiband squared envelope spectrum method integrates spectrum information across multiple frequency bands to reduce the bias caused by single-band selection [12]; however, it requires empirical band division, which increases the computational load. The neural network-based spectrum analysis can improve feature extraction at low signal-to-noise ratio conditions [13]; but it highly depends on the quality of training data sets. Multiple correlation analysis selects representative intrinsic mode functions (IMFs) using combined correlation indicators [14]; but its performance still depends on the quality of variational mode decomposition (VMD). Parameter-adaptive variational mode decomposition (VMD) methods aim to optimize the number of decomposition modes and penalty factors to improve the extraction of fault-related components. An improved parameter-adaptive VMD method based on maximum average envelope kurtosis has been proposed to reduce over-decomposition and under-decomposition; however, its iterative parameter optimization increases computational complexity [15]. Energy-constrained swarm decomposition and adaptive spectral amplitude modulation [16] provide alternative adaptive frameworks; but they involve multi-level iterative optimization, convergence is sensitive to initialization. Signal decomposition techniques, such as EMD [17], local mean decomposition [18] and VMD [14], can be used to decompose vibration signals into several intrinsic components over different frequency bands, thereby separating fault-related pulses from strong background interference. Nonetheless, these methods produce many modes that complicate subsequent analysis; furthermore, it is usually challenging to distinguish the informative mode from redundant modes [19].

In recent years, a chirp mode decomposition (CMD) method has been used for non-stationary and nonlinear signal analysis. It can extract the most informative amplitude/frequency modulated (AM/FM) components during each iteration [20]. Instead of producing multiple modes, the CMD generates one dominant component at each decomposition step; this component is then modeled as a narrowband AM-FM signal whose energy is concentrated around a time-varying center frequency. The CMD can update instantaneous amplitude (IA) and instantaneous phase (IP) alternately during iteration by minimizing a cost function that constrains both component bandwidth and structural smoothness. By repeatedly optimizing IA and IP, the CMD can properly track the frequency variation and chirp characteristics in machine vibration signals. In recent years, several studies have attempted to improve CMD for bearing fault detection [21]. For example, a joint adaptive signal decomposition technique uses CMD to analyze the signal constructed by VMD. However, it needs to optimize two sets of parameters with enlarged searching spaces and prone to local minima [22]. A modified CMD in [23] involves relatively complicated processing, and its stability may not be guaranteed under different operating conditions. Furthermore, these CMD variants

mainly focus on improving the extraction quality of the mode itself, without clear improvement in representative feature recognition. Advanced investigation shows that noise and interference can introduce excessive spectral details and obscure the true periodic impact signatures in the envelope spectrum [24].

To tackle the above limitations, an enhanced CMD (eCMD) technique will be proposed in this work for more reliable signal property analysis and for bearing fault detection. The eCMD technique has the following novelty points: 1) The expected bearing fault trajectories are used to provide clear physical justification for signal decomposition. 2) An envelope demodulation approach is suggested to suppress noise and interference and highlight the second-order cyclic impact features for bearing fault detection. The effectiveness of the eCMD technique will be evaluated by experimental tests corresponding to different bearing conditions.

The remainder of this paper is organized as follows: the proposed eCMD technique is presented in Section 2. The effectiveness of the eCMD technique is verified in Section 3 by experiential tests. Some concluding remarks are summarized in Section 4.

2. The Proposed eCMD Technique

The proposed eCMD technique aims to extract representative features from vibration signals for signal property analysis and bearing fault detection. The processing procedures of the eCMD are illustrated in **Figure 2**. Details will be discussed in the following subsections.

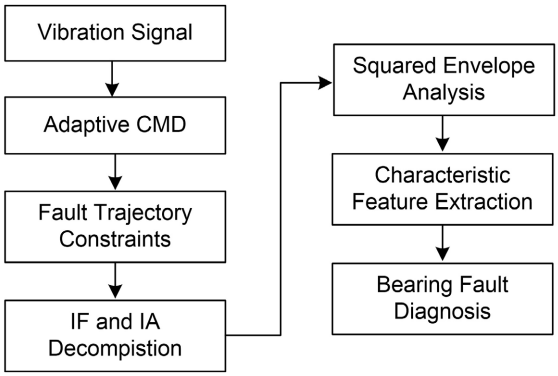

Figure 2. Flowchart of the proposed eCMD technique.

2.1. CMD Analysis

The vibration signal collected from rolling element bearings can be modeled as a nonlinear and non-stationary amplitude modulation-frequency modulation (AM-FM) signal with time-varying amplitudes and frequencies. Based on this model, the adaptive CMD decomposes the signal based on an optimization framework to extract the most representative mode [23]. Given a vibration signal $x(t)$, the i-th component can be expressed as

$$x_i(t) = A_i(t)\cos\left(2\pi\int_0^t f_i(s)\mathrm{d}s + \phi_i\right) \quad (1)$$

where $A_i(t)$ and $f_i(t)$ denote the instantaneous amplitude and instantaneous frequency, respectively; and ϕ_i is the initial phase at $t = 0$.

2.2. Bearing Characteristic Frequencies

The bearing fault characteristic frequencies depend on the geometric parameters of the bearing [3]. When periodic impacts in the vibration match a characteristic frequency or its harmonic, resonance occurs. The resonance features will be used for bearing fault detection and fault type diagnosis [7] [8]. Consider a rolling element bearing with a pitch diameter D, rolling element diameter d, angle of contact θ, and Z rolling elements, as illustrated in **Figure 1**. If the instantaneous shaft (or inner race) rotating frequency is f_r Hz, the respective characteristic frequencies if the defect occurs on the outer race (f_{OD}), the inner race (f_{ID}), and a rolling element (e.g., a ball) (f_{BD}) will be [9]:

$$f_{OD} = \frac{Z}{2}\left(1 - \frac{d}{D}\cos\theta\right)\cdot f_r \tag{2}$$

$$f_{ID} = \frac{Z}{2}\left(1 + \frac{d}{D}\cos\theta\right)\cdot f_r \tag{3}$$

$$f_{BD} = \frac{D}{2d}\left[1 - \left(\frac{d}{D}\cos\theta\right)^2\right]\cdot f_r \tag{4}$$

Instead of searching for the chirp rate best fitting the signal as in most decomposition techniques [20] [21], the proposed eCMD looks for instantaneous frequency evolution being physically possible for this bearing fault. This can provide clear physical justification for the adaptive CMD operation, rather than treating the chirp rate as an arbitrary signal processing parameter. The instantaneous chirp rate will be:

$$c_i(t) = \frac{\mathrm{d}f_i(t)}{\mathrm{d}t} \tag{5}$$

2.3. Adaptive CMD Operation

In processing, the continuous-time vibration signal $x(t)$ can be written as

$$x(t) = \sum_{i=1}^{M} x_i(t) + \delta(t) \tag{6}$$

where $M \in N^+$ is the number of AM-FM components, and $\delta(t)$ represents the noise.

The demodulated phase function $\tilde{\phi}_i(t)$ is defined by introducing an estimated initial frequency term $\tilde{f}_i(t)$ such that

$$\tilde{\phi}_i(t) = 2\pi\int_0^t \tilde{f}_i(s)\mathrm{d}s \tag{7}$$

The phase difference $\Delta\phi_i(t)$ is defined to iteratively correct the estimated instantaneous frequency to gradually approach the true instantaneous frequency:

$$\Delta\phi_i(t) = 2\pi\int_0^t \left(f_i(s) - \tilde{f}_i(s)\right)\mathrm{d}s + \phi_i \tag{8}$$

The *i*-th signal component can be written in a demodulated sinusoidal form:

$$x_i(t) = a_i(t)\cos\left(\phi_i(t)\right) - b_i(t)\sin\left(\phi_i(t)\right) \tag{9}$$

$$a_i(t) = A_i(t)\cos\left(\Delta\phi_i(t)\right) \tag{10}$$

$$b_i(t) = A_i(t)\sin\left(\Delta\phi_i(t)\right) \tag{11}$$

where $a_i(t)$ and $b_i(t)$ represent in-phase and quadrature components of $x_i(t)$. Accordingly, the instantaneous amplitude can be expressed as

$$A_i(t) = \sqrt{a_i^2(t) + b_i^2(t)} \tag{12}$$

If the estimated instantaneous frequency matches the true instantaneous frequency, or $\tilde{f}_i(t) \approx f_i(t)$, the residual FM is negligible. As a result, the demodulated $x_i(t)$ can be approximated as an AM signal. Accordingly, the in-phase and quadrature components of $x_i(t)$ can be approximated as

$$a_i(t) \approx A_i(t)\cos\left(\phi_i\right) \tag{13}$$

$$b_i(t) \approx A_i(t)\sin\left(\phi_i\right) \tag{14}$$

Thus, the problem of estimating the instantaneous amplitude and instantaneous frequency by minimizing the residual FM can be formulated as a regularized least-squares estimation problem with the following objective function:

$$\min_{a_i,b_i,\phi_i} \int\left(x(t) - \sum_{i=1}^{M} x_i(t)\right)^2 \mathrm{d}t + \lambda\int\left[\left(\frac{\mathrm{d}^2 a_i(t)}{\mathrm{d}t^2}\right)^2 + \left(\frac{\mathrm{d}^2 b_i(t)}{\mathrm{d}t^2}\right)^2\right]\mathrm{d}t \tag{15}$$

where λ is the amplitude smoothness parameter. The term $\int\left(x(t) - \sum_{i=1}^{M} x_i(t)\right)^2 \mathrm{d}t$ is to prevent excessive deviation from observed data in reconstructing the signal $x(t)$ using to the decomposed components. The term $\int\left[\left(\frac{\mathrm{d}^2 a_i(t)}{\mathrm{d}t^2}\right)^2 + \left(\frac{\mathrm{d}^2 b_i(t)}{\mathrm{d}t^2}\right)^2\right]\mathrm{d}t$ is to smooth envelopes by penalizing rapid variations (high curvature) in the envelope functions $a_i(t)$ and $b_i(t)$. $\lambda \in \left[10^{-8}, 10^{-1}\right]$ scales the second-order difference penalty of the demodulated signal amplitudes. A small λ allows the amplitude to fluctuate rapidly to fit the signal spikes, resulting in a low noise regulation (under-smoothing). In contrast, a large λ has a higher noise regulation, filtering out sharp amplitude fluctuations or transient features from the output (over smoothing) [25]. Specifically, $\lambda \in \left[10^{-3}, 10^{-1}\right]$ is used if the noise level is high; increasing λ can suppress noise ripples in the amplitude. Otherwise, $\lambda \in \left[10^{-8}, 10^{-4}\right]$ is used if the noise level is low. Decreasing λ helps capture intricate physical amplitude modulations. In the following tests, $\lambda = 10^{-3}$ is used.

By minimizing Equation (15), the instantaneous frequency estimate is iteratively refined to reduce residual frequency modulation. It also ensures the extracted component exhibiting minimal residual FM with smooth envelopes to make $f_i(t) - \tilde{f}_i(t) \to 0$. To solve Equation (15) numerically, the continuous signal $x(t)$ is sampled at a sampling frequency f_s, yielding a discrete time sequence

$x[n]$, represented in a vector form:

$$x[n]=\left[x(t_0),x(t_1),\cdots,x(t_{N-1})\right]^{\mathrm{T}},\ n=0,1,2,\cdots,N-1 \tag{16}$$

where $t_n=n\Delta t$, $\Delta t=1/f_s$; and N is the total number of discrete samples.

The continuous envelope functions $a_i(t)$ and $b_i(t)$ can be discretized as vectors $a_i[n]$ and $b_i[n]$, respectively. Then, Equation (9) can be rewritten in the following matrix form

$$\boldsymbol{x}_i=M_{c,i}\cdot\boldsymbol{a}_i+M_{s,i}\cdot\boldsymbol{b}_i=B_i\boldsymbol{p}_i \tag{17}$$

where $M_{c,i}$ and $M_{s,i}$ are diagonal matrices constructed from the respective cosine and sine functions of the demodulated phase sequences, such that

$$M_{c,i}=\mathrm{diag}\begin{bmatrix}\cos(\varphi_i(t_0))\\ \cos(\varphi_i(t_1))\\ \vdots\\ \cos(\varphi_i(t_{N-1}))\end{bmatrix},\quad M_{s,i}=\mathrm{diag}\begin{bmatrix}\sin(\varphi_i(t_0))\\ \sin(\varphi_i(t_1))\\ \vdots\\ \sin(\varphi_i(t_{N-1}))\end{bmatrix} \tag{18}$$

where N is the number of discrete samples, and φ_i denotes the discrete demodulated phase sequence.

Let $P_i=\left[a_i^{\mathrm{T}},b_i^{\mathrm{T}}\right]^{\mathrm{T}}$ and $B_i=\left[M_{c,i},M_{s,i}\right]\in R^{N\times 2N}$, then Equation (17) can be rewritten as

$$x_i=B_iP_i \tag{19}$$

The second-order derivative of the envelope function is approximated using a second-order finite difference scheme:

$$\Delta^2a_i(t_n)\approx a_i(t_{n+1})-2a_i(t_n)+a_i(t_{n-1}) \tag{20}$$

where $\Delta^2(\cdot)$ denotes the second-order discrete difference operator. Accordingly, a second-order discrete difference operator D can be defined as

$$D=\begin{bmatrix}1&-2&1&0&\cdots&0\\ 0&1&-2&1&\cdots&0\\ \vdots&&&\ddots&&\vdots\\ 0&\cdots&0&1&-2&1\end{bmatrix}_{(N-2)\times N} \tag{21}$$

Then $D\in R^{(N-2)\times N}$ can be applied to the in-phase and quadrature components $a_i[n]$ and $b_i[n]$; and $\eta\in R^{(2N-4)\times 2N}$ is a block-diagonal operator defined as

$$\eta=\begin{bmatrix}D&0\\ 0&D\end{bmatrix} \tag{22}$$

Then the smoothness regularization term $\int\left[\left(\frac{\mathrm{d}^2a_i(t)}{\mathrm{d}t^2}\right)^2+\left(\frac{\mathrm{d}^2b_i(t)}{\mathrm{d}t^2}\right)^2\right]\mathrm{d}t$ is approximated in the discrete domain as $\left\|\eta P_i\right\|_2^2$, where the second-order difference operator provides a finite-difference approximation of the continuous derivatives. After discretization, Equation (15) can be reformulated as a regularized least squares problem in the discrete domain:

$$J = \left\| \eta P_i \right\|_2^2 + \mu \left\| x - B_i P_i \right\|_2^2 \tag{23}$$

where x denotes the discrete-time vibration signal obtained by sampling the continuous signal $x(t)$; μ is the weigh coefficient. The cost function can be expanded to

$$J_i = P_i^{\mathrm{T}} \eta^{\mathrm{T}} \eta P_i + \mu \left(x^{\mathrm{T}} x - 2 x B_i P_i + P_i^{\mathrm{T}} B_i^{\mathrm{T}} B_i P_i \right). \tag{24}$$

The optimal solution of P_i is obtained by setting $\partial J_i / \partial P_i = 0$, or

$$P_i^j = \left(\frac{1}{\mu} \eta^{\mathrm{T}} \eta + \left(B_i^j \right)^{\mathrm{T}} B_i^j \right)^{-1} B_i^{\mathrm{T}} x \tag{25}$$

The signal component and its IA are then updated as:

$$x_i^j = B_i^j P_i^j \tag{26}$$

$$A_i^j [n] = \sqrt{\left(a_i^j [n] \right)^2 + \left(b_i^j [n] \right)^2} \tag{27}$$

The instantaneous frequency is updated by solving the following optimization problem

$$\min \quad \left\| f_i^{j+1} - f_i^j - \Delta \tilde{f}_i^j \right\|_2^2 + \frac{1}{\gamma} \left\| D f_i^{j+1} \right\|_2^2 \tag{28}$$

where $\gamma \in \left[10^{-5}, 10^{-1} \right]$ is the frequency smooth parameter. It scales the penalty on the variations of the instantaneous frequency. If γ decreases, the estimated instantaneous frequency becomes overly smooth, failing to track highly non-stationary or rapidly changing chirps. In contrast, if γ increases, the tracking becomes hyper-sensitive, capturing noise fluctuations or oscillating wildly [25]. Specifically, $\gamma \in \left[10^{-2}, 10^{-1} \right]$ is used if it is highly nonlinear; increasing γ allows the algorithm to follow steep frequency changes. $\gamma \in \left[10^{-5}, 10^{-3} \right]$ is used if it is not very nonlinear; decreasing γ keeps the instantaneous frequency track smooth and stable. In the following tests, $\gamma = 10^{-4}$ is used.

If the residual term $\left\| f_i^{j+1} - f_i^j - \Delta \tilde{f}_i^j \right\|_2^2$ in Equation (28) is non-trivial, the iterative update of the instantaneous frequency will minimize this residual. By setting the first derivative of the objective function Equation (28) with respect to f_i^{j+1} and letting it to zero, the instantaneous frequency is updated as:

$$f_i^{j+1} = f_i^j + \left(\frac{1}{\gamma} D^{\mathrm{T}} D + I \right)^{-1} \Delta \tilde{f}_i^j \tag{29}$$

where $I \in R^{N \times N}$ is an identity matrix.

The updated instantaneous frequency is then to obtain the new phase function

$$\phi_i^{j+1} [n] = 2\pi \sum_{k=0}^{n} f_i^{j+1} [k] \tag{30}$$

The iteration is terminated when the following condition is satisfied

$$\frac{\left\| \boldsymbol{P}_i^{j+1} - \boldsymbol{P}_i^j \right\|_2}{\left\| \boldsymbol{P}_i^j \right\|_2 + \varepsilon} \le T_C \tag{31}$$

where ε is a small positive constant introduced to avoid division by zero. T_C is a predefined convergence tolerance. $T_C = 10^{-5}$ is selected in this work to balance convergence accuracy and computational efficiency. Another stopping criterion is the maximum iteration limit of 200 interactions. This hard cutoff number of iterations is included to prevent infinite loops if the algorithm encounters noisy, highly non-stationary sections that struggle to converge.

Finally, the extracted mode $x_i[n]$ is reconstructed using Equation (9). Its instantaneous amplitude $A_i[n]$ are computed according to Equation (12).

2.4. Enhanced Envelope Analysis

The amplitude sequence $A_i[n]$ obtained from the previous CMD contains representative features related to bearing fault impulses, as well as irrelevant modes and noise [24] [26]. Therefore, compared with the original vibration signal $x(t)$, the extracted amplitude sequence will be used for envelope analysis to recognize representative features. The pre-whitening processing [19] is applied to $A[n]$ to suppress deterministic components such as shaft-related and motor-related features and their harmonics by

$$A_w[n] = \Re\left\{F^{-1}\left(\frac{X_A[f]}{|X_A[f]|+\varepsilon}\right)\right\} \tag{32}$$

where $X_A[f]$ denotes the Fourier spectrum of the amplitude sequence $A[n]$; ε is a small constant number introduced for numerical stability to prevent division by zero; $\Re\{\cdot\}$ denotes the real part; and $F^{-1}(\cdot)$ denotes the inverse discrete FT.

Equation (32) represents a Cepstrum pre-whitening operation. A rotating machine produces strong, periodic, multi-harmonic deterministic components of shaft rotating speeds. Meanwhile, localized bearing defects generate transient, impulsive shocks that are cyclostationary rather than strictly periodic. A cepstrum map can recognize peaks at "quefrencies" that correspond to the period of these periodic base frequencies. In the pre-whitening operation, the real part of the cepstrum is zeroed out, or the FT signal is divided by its absolute value. When transformed back to the time or frequency domain, this pre-whitening process can "whiten" the background noise and remove strong periodic/harmonic excitations and resonance peaks. As a result, weaker impulsive features caused by bearing fault could be highlighted during subsequent envelope analysis.

The next step is to band-pass filter the pre-whitened amplitude sequence $A_w[n]$ in the frequency domain [27] to recognize the relevant modulation components of the amplitude sequence:

$$A_f[n] = F^{-1}\left\{F\left(A_w[n]\right)W[k]\right\} \tag{33}$$

The discrete frequency indices are defined as

$$l = \left(f_l/f_s\right)L, \quad h = \left(f_h/f_s\right)L \tag{34}$$

where f_l and f_h in Hz denote the lower and upper cutoff frequencies of the band-pass filter; f_s is the sampling frequency; and L is the signal length. $W[k]$ is the

band-pass filter defined over the bandwidth [*l*, *h*].

The amplitude sequence $A_f[n]$ can be approximated as a quasi-periodic signal expressed as a finite Fourier series:

$$A_f[n] \approx a_0 + \sum_{k=1}^{K} A_k \cos\left(2\pi k f_c n / f_s + \phi_k\right) \tag{35}$$

where a_0 denotes the mean value of the amplitude sequence; A_k represents the amplitude of the *k*-th harmonic; f_c is the characteristic frequency of the bearing fault; and φ_k is the corresponding phase.

Squared envelope $e[n] = \left|A_f[n]\right|^2$ will be applied to enhance the periodic components related to the impacts and the fault-related modulation frequencies in the spectral domain. The squared envelope will be expanded as

$$\begin{aligned} e[n] &= \left|A_f[n]\right|^2 \\ &= a_0^2 + \frac{1}{2}\sum_k A_k^2 + 2a_0 \sum_k A_k \cos\left(2\pi k f_c n / f_s + \theta_k\right) + \frac{1}{2}\sum_k A_k^2 \cos\left(4\pi k f_c n / f_s + 2\theta_k\right) \\ &\quad + \frac{1}{2}\sum_k \sum_l A_k A_l \left[\cos 2\pi\left(k-l\right) f_c n / f_s + \cos 2\pi\left(k+l\right) f_c n / f_s\right], \end{aligned} \tag{36}$$

where A_k is the amplitude of the *k*-th harmonic component associated with the bearing fault with characteristic frequency f_c; $k, l = 1, 2, 3, \ldots, |k - l| = 0, 1, 2, \ldots$ denote the harmonic indices of f_c. The effective ranges of *k* and *l* are determined by the selected bandwidth corresponding to different bearing health conditions. For example, if the bandwidth of interest is up to 400 Hz, and the characteristic frequency $f_c = 50$ Hz, indices *k* and *l* will be up to $400/f_c = 8$.

The squared envelope spectrum can be obtained by taking the FT of the squared envelope sequence $e[n]$. Bearing fault detection and fault type diagnosis are performed by examining the fault-related characteristic frequenc f_c and its harmonics. A normalized spectral indicator at each characteristic frequency and its harmonics is defined as:

$$R(f_c) = \frac{S(f_c)}{\sigma_S} \tag{37}$$

where $S(f_c)$ represents the squared envelope spectrum amplitude at f_c; and σ_S is the standard deviation of the envelope spectrum amplitudes within the analysis band.

3. Performance Evaluation and Test Analysis

The effectiveness of the proposed eCMD technique is verified in this section using experimental tests corresponding to different bearing conditions.

3.1. Methods for Comparison

For comparison, the performance of the proposed eCMD technique is evaluated against several related and well-accepted CMD techniques for bearing fault detection:

1) Adaptive CMD, ACMD in short, is a signal processing technique used to decompose signals into individual intrinsic chirp components while simultaneously estimating their instantaneous frequencies and amplitudes for bearing fault detection [20].

2) Scale-demodulation CMD, SCMD in short, is a fault detection technique that can extract subtle impulse and modulation components from vibration signals for bearing fault detection under non-stationary operating conditions [8].

3) Joint CMD, JCMD in short, is a VMD-based CMD method, which is an adaptive signal decomposition method aiming to improve fault feature extraction from weak and non-stationary vibration signals [22].

All the techniques are implemented in MATLAB 2022b. To make a fair comparison, the initial parameters of these four CMD algorithms are selected compatibly. The selection of some related parameters, such as the amplitude smoothness parameter, frequency smooth parameter, and predefined convergence tolerance, has been discussed in Subsection 2.3. Other related initial parameters are selected such as: filter bandwidth of 1000 - 8000 Hz (fourth order Butterworth); maximum extracted modes: 6; residual energy stopping threshold: 0.05, etc.

3.2. Experimental Setup

Figure 3 shows the experimental setup used in this test. It is driven by a 3 HP electric motor with a speed range of 100 - 4200 rpm, controlled by a frequency converter. An elastic coupler is applied to eliminate high frequency vibrations generated by the motor. An optical sensor is used to provide a one-pulse-per-revolution signal to estimate shaft speed. The accelerometers are mounted on the top and back of the bearing housing to measure the vibration signals along different directions. The vibration signals are fed to a computer through a smart data acquisition board developed by our research team. The tested bearing (MBER-10K) is located on the left side of the housing. The static bearing load is provided by two heavy mass discs and dynamic load is provided by a brake system through a belt-drive.

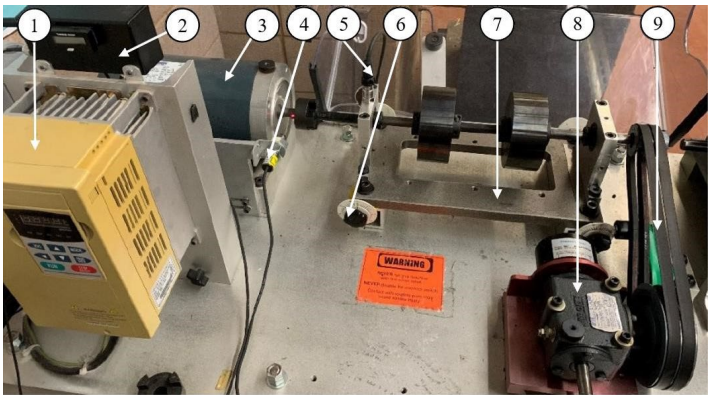

Figure 3. Experimental setup: (1) speed control; (2) encoder display; (3) drive motor; (4) optical encoder; (5) ICP accelerometer; (6) misalignment adjustor; (7) adjustable rig; (8) variable load system; (9) belt drive.

A series of data sets have been collected from multiple accelerometers mounted on both sides of the bearing housing. The vibration signals measured by the vertical accelerometer mounted closest to the tested bearing (left side of the bearing housing) are used for subsequent signal processing and analysis. The tested bearing health conditions include healthy bearings, bearings with outer race, inner race and rolling element defects, respectively. The defect dimension (in diameter × depth) is: 0.3 mm × 0.3 mm for outer race defect, 0.3 mm × 0.3 mm for inner race defect, and 0.5 mm × 0.5 mm for a ball defect, respectively.

The tests are undertaken over shaft speed of 100 - 4200 rpm. The load levels are over 0.5 - 2 Nm: light load (0.5 - 1.0 Nm), medium load (1.0 - 1.5 Nm) and heavy load (1.5 - 2.0 Nm), respectively.

A set of processing results from tests with 1800 rpm (or $f_r = 30$ Hz) and medium load level are used for illustration. The sampling frequency is 32,000 Hz, and the length of the signal is 100 k.

In this experiment, the tested bearings have the following parameters: Number of rolling elements (balls) $Z = 8$; Rolling element diameter $d = 7.938$ mm; Pitch diameter $D = 33.503$ mm; Contact angle $\theta = 0$ degrees. Using Equations (2)-(4), the characteristic frequencies in terms of shaft speed f_r Hz are calculated and summarized in Table 1.

Table 1. Bearing fault frequencies in terms of shaft speed f_r Hz.

Bearing Health Condition	Characteristic Frequency (Hz)
Healthy bearing	$f_H = f_r$
Outer race fault	$f_{OR} = 3.052 \times f_r$
Inner race fault	$f_{IR} = 4.948 \times f_r$
Rolling element fault	$f_{BD} = 1.992 \times f_r$

3.3. Test Result Analysis

3.3.1. Healthy Bearing Analysis

For the healthy bearing condition, the characteristic frequency is the shaft rotating frequency $f_H = f_r = 30$ Hz. Figure 4 shows the processing results using the related techniques. The ACMD in Figure 4(a) can recognize f_H and its harmonics over the bandwidth of [0, 400] Hz. But its 3rd harmonic is the dominant spectral component due to its overlapping instantaneous frequencies. The SCMD in Figure 4(b) has a dominant f_H and a series of harmonics due to its improved mode separation. JCMD in Figure 4(c) has a dominant 6th harmonic of f_H, but other characteristic frequency harmonics are attenuated by noise. The proposed eCMD technique in Figure 4(d), however, can capture the characteristic frequency f_H clearly with suppressed noise due to its efficient mode decomposition and envelope demodulation. It produces the clearest and most structured spectrum, reflecting a clearer representation of the characteristic frequency for a healthy bearing.

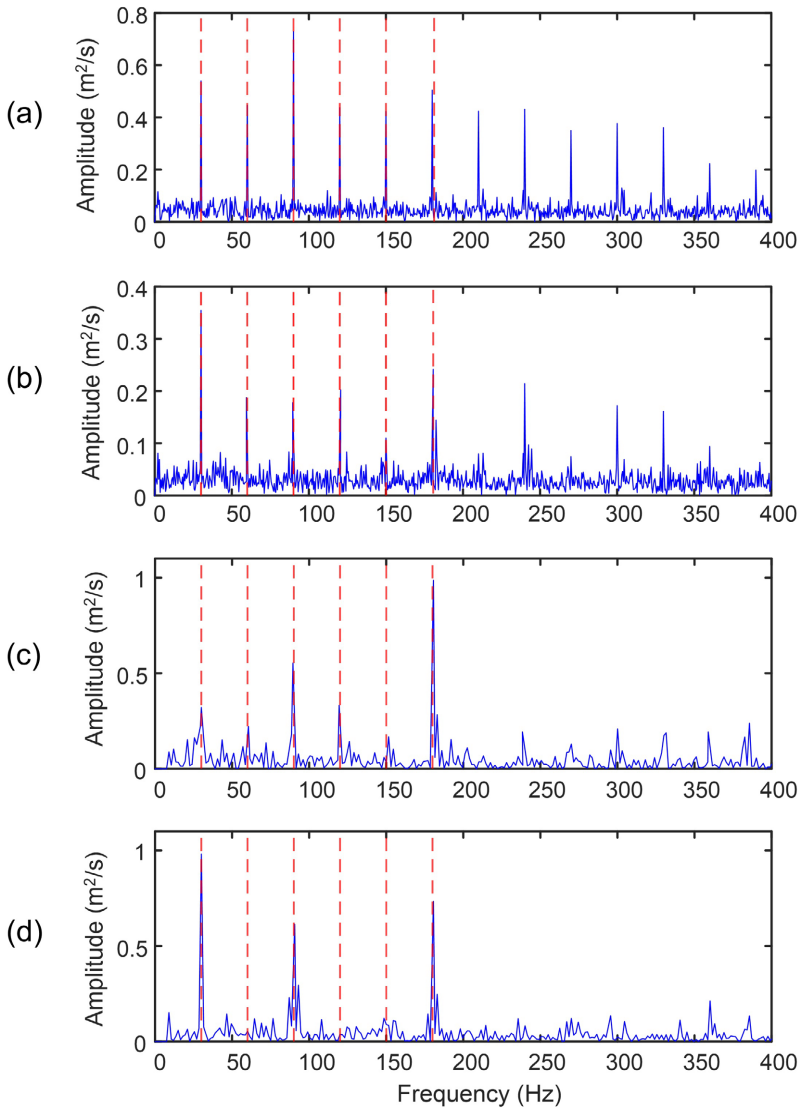

Figure 4. Processing result comparison for a healthy bearing using the related techniques: (a) ACMD, (b) SCMD, (c) JCMD, (d) the proposed eCMD. The red dashed lines denote the bearing characteristic frequency (f_H = 30 Hz) and its harmonics.

3.3.2. Outer Race Bearing Fault Detection

For the outer race fault case, the characteristic frequency is f_{OR} = 91.6Hz. As illustrated in **Figure 5(a)**, the ACMD can recognize the 2nd harmonic of f_{OR}; however, it is not the dominant frequency component on the spectrum, which can generate false diagnosis. The dominant spectral component at 84.1 Hz is associated with a system resonant frequency component. Although SCMD in **Figure 5(b)** has a dominant 2nd harmonic of f_{OR}, it exhibits relatively dispersed spectral energy due to over-decomposition. JCMD in **Figure 5(c)** can enhance the periodic impact signatures associated with the outer-race defect. Its dominant frequency component is the 3rd harmonic of f_{OR} with noticeable spectral leakage. In contrast, the proposed eCMD technique in **Figure 5(d)** shows clearer harmonic alignment and the best compact spectral representation due to its efficient chirp decomposition

and mode separation.

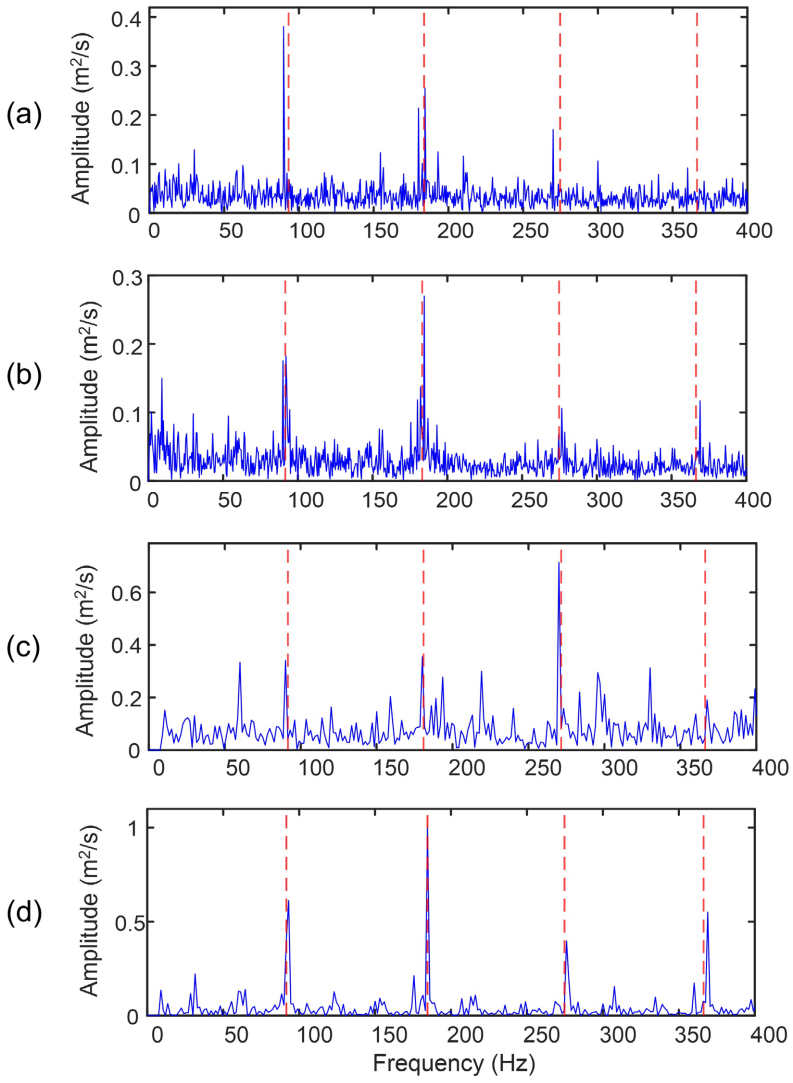

Figure 5. Processing result comparison for a bearing with outer race fault using the related techniques: (a) ACMD, (b) SCMD, (c) JCMD, (d) the proposed eCMD. The red dashed lines denote the bearing characteristic frequency (f_{OR} = 91.6 Hz) and its harmonics.

3.3.3. Inner Race Bearing Fault Detection

For the inner race fault case, the characteristic frequency is f_{IR} = 148.4Hz. Both ACMD in **Figure 6(a)** and KCMD in **Figure 6(b)** can recognize the occurrence of the inner race fault with the dominant spectral component of f_{IR}. However, their high background noise is due to signal modulations generated during the decomposing process. Although JCMD in **Figure 6(c)** can recognize the 2nd and 3rd harmonics of f_{IR}, they are not the dominant spectral components due to spectral spreading and noise interference. In comparison, eCMD in **Figure 6(d)** can effectively suppress noisy spectral components, resulting in a more compact and interpretable harmonic structure, due to its effective chirp decomposition and enhanced squared envelope analysis.

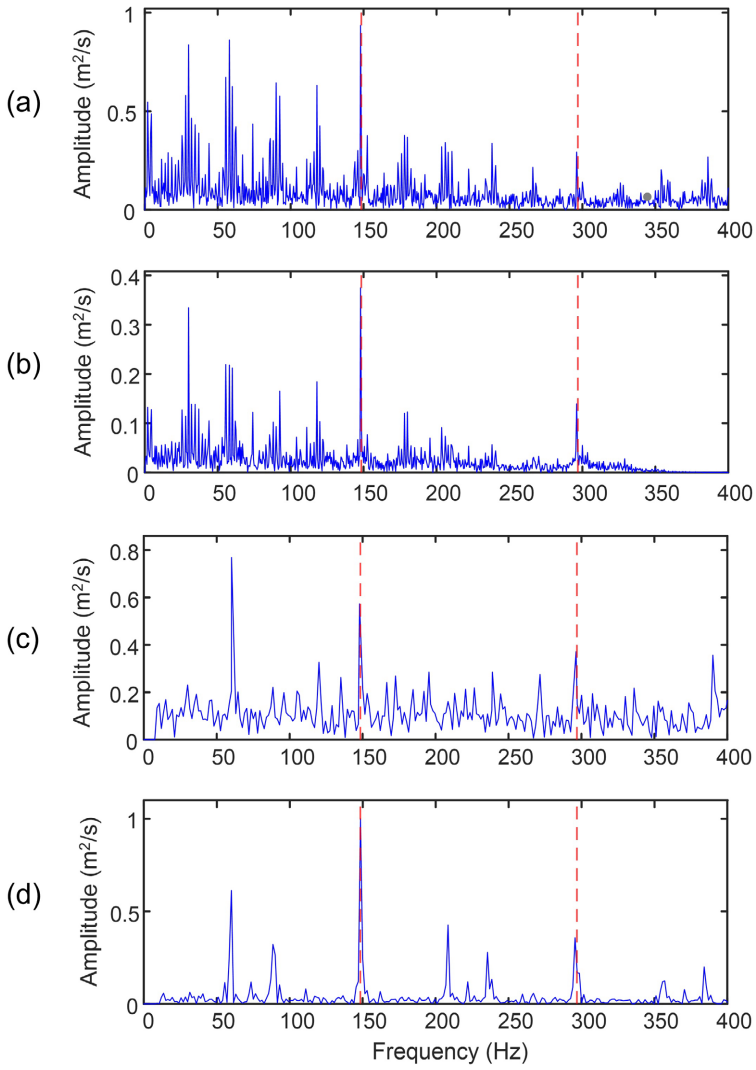

Figure 6. Processing result comparison for a bearing with inner race fault using the related techniques: (a) ACMD, (b) SCMD, (c) JCMD, (d) the proposed eCMD. The red dashed lines denote the bearing characteristic frequency (f_{IR} = 148.4 Hz) and its harmonics.

3.3.4. Rolling Element Bearing Fault Detection

For the rolling-element (a ball in this case) fault condition, the characteristic frequency is f_{BD} = 59.7 Hz using the bearing geometry and shaft rotational speed. As illustrated in **Figure 7**, the envelope spectra from all methods exhibit less distinct representative features compared with race faults. None of these techniques can clearly recognize the ball fault. When a ball is damaged, its generated impact vibration features vary with time, because the damaged ball location may not always strike the races. This phenomenon is characterized by continuously varying contact conditions and non-stationary impulsive responses. As a result, the corresponding fault features tend to be weaker, less periodic, and more difficult to isolate in spectrum analysis. From the spectral plots, ball fault exhibits dispersed energy and limited harmonic continuity. Although none of these four methods can clearly identify the ball fault, the proposed eCMD technique in **Figure 7(d)** pro-

vides a relatively more concentrated spectral response around the characteristic frequency and its 3rd harmonic due to its more efficient chirp decomposition and envelope demodulation. Advanced research is required to develop new techniques for bearing rolling element fault detection.

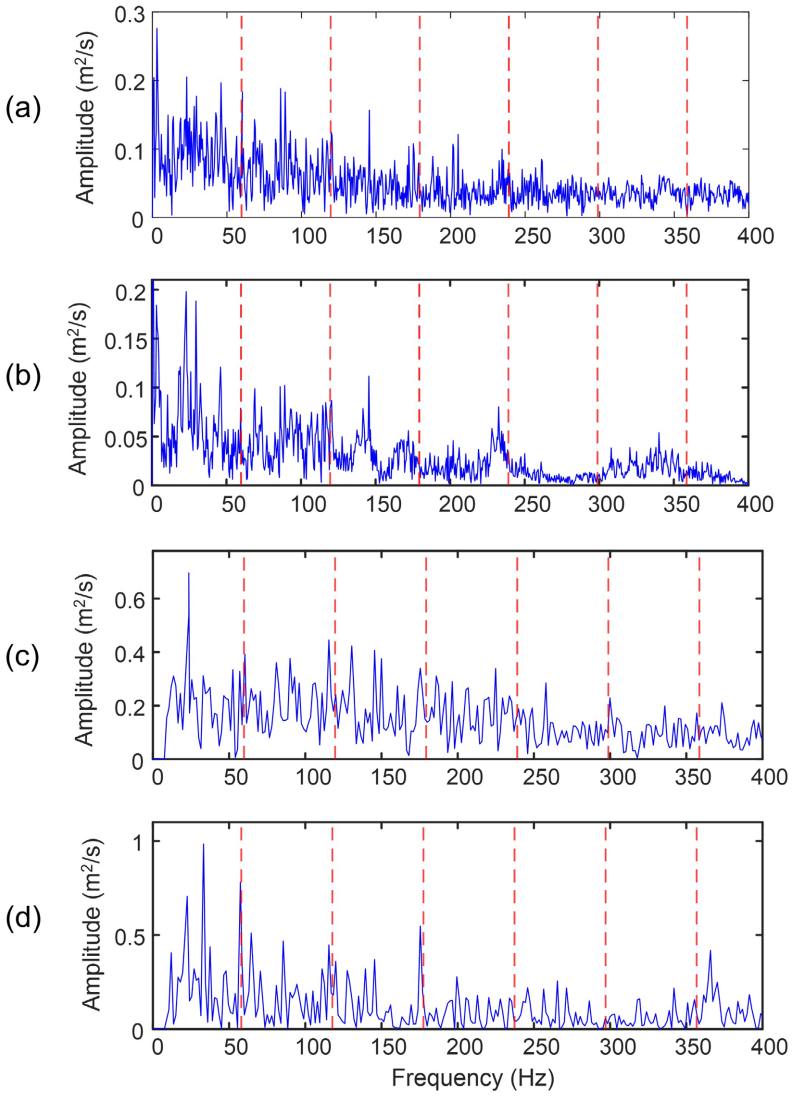

Figure 7. Processing result comparison for a bearing with rolling-element fault using the related techniques: (a) ACMD, (b) SCMD, (c) JCMD, (d) the proposed eCMD. The red dashed lines denote the bearing characteristic frequency (f_{BD} = 59.7 Hz) and its harmonics.

4. Conclusions

Reliable fault detection in rolling element bearings remains a challenging task, especially in real-world automatic machine condition monitoring. A new enhanced chirp mode decomposition, eCMD, technique has been proposed in this work for nonlinear signal property analysis and bearing fault detection. The eCMD has two main processing procedures: 1) The adaptive CMD is used to extract the dominant instantaneous amplitude and frequency. Bearing fault frequency trajectories

are introduced to estimate both instantaneous frequency and chirp rate of each mode. The purpose is to provide clear physical justification for the adaptive chirp rate estimation. 2) An envelope demodulation approach is suggested to suppress noise and enhance the second-order cyclic impact features for bearing fault detection and fault type diagnosis. The effectiveness of the proposed eCMD technique has been examined by experimental tests under different bearing health and operating conditions. Test results have shown that the eCMD technique can improve the reliability of fault feature extraction from non-stationary vibration signals, without relying on manual mode selection or explicit noise modeling. It can provide better spectral representation of fault characteristic frequencies for bearing fault detection and fault type diagnosis. It has potential to be used as an input for the real-world machine health condition monitoring.

Advanced research will be undertaken for the following issues: 1) A new approach will be proposed for bearing ball fault detection. 2) Automated optimization method will be proposed to adaptively update the related parameters in the eCMD algorithm.

Acknowledgements

This work is supported in part by Natural Sciences and Engineering Research Council of Canada (NSERC), and Bare Point Water Treatment Plant in Thunder Bay, ON, Canada.

Author Contributions

Conceptualization, R.Z., M.M., W.W; methodology, M.M. R.Z., W.W.; software, M.M.; R.Z.; validation, R.Z., M.M.; formal analysis, R.Z., M.M., W.W.; investigation, M.M., R.Z.; resources, W.W.; data curation, R.Z., M.M.; writing—original draft preparation, R.Z.; M.M.; writing—review and editing, W.W.; visualization, R.Z., M.M.; supervision, W.W.; project administration, W.W.; funding acquisition, W.W. All authors have read and agreed to the published version of the manuscript.

Conflicts of Interest

The authors declare no conflicts of interest regarding the publication of this paper.

References

[1] Xing, X., Zhang, M., Wang, W. and Melek, W. (2026) A Smart Sensor-Based Bearing Fault Detection Technology. *IEEE/ASME Transactions on Mechatronics*, **31**, 3370-3381. https://doi.org/10.1109/tmech.2025.3644347

[2] Cui, L., Sun, Y., Wang, X. and Wang, H. (2021) Spectrum-Based, Full-Band Preprocessing, and Two-Dimensional Separation of Bearing and Gear Compound Faults Diagnosis. *IEEE Transactions on Instrumentation and Measurement*, **70**, Article 3513216. https://doi.org/10.1109/tim.2021.3063189

[3] Malusare, M., Mahmud, M. and Wang, W. (2025) An Enhanced TK Technology for Bearing Fault Detection Using Vibration Measurement. *Sensors*, **25**, Article No. 6571.

https://doi.org/10.3390/s25216571

[4] Cheng, Z. and Wang, R. (2020) Enhanced Symplectic Characteristics Mode Decomposition Method and Its Application in Fault Diagnosis of Rolling Bearing. *Measurement*, **166**, Article ID: 108108. https://doi.org/10.1016/j.measurement.2020.108108

[5] Xing, X., Wang, W. and Melek, W. (2026) A New Swarm Decomposition Technique for Bearing Fault Detection and Diagnosis. *IEEE Transactions on Instrumentation and Measurement*, **75**, Article ID: 3508213. https://doi.org/10.1109/tim.2026.3667340

[6] Ma, J., Zhuo, S., Li, C., Zhan, L. and Zhang, G. (2021) An Enhanced Intrinsic Time-Scale Decomposition Method Based on Adaptive Lévy Noise and Its Application in Bearing Fault Diagnosis. *Symmetry*, **13**, Article No. 617. https://doi.org/10.3390/sym13040617

[7] Meng, J., Wang, H., Zhao, L. and Yan, R. (2021) Compound Fault Diagnosis of Rolling Bearing Using PWK-Sparse Denoising and Periodicity Filtering. *Measurement*, **181**, Article ID: 109604. https://doi.org/10.1016/j.measurement.2021.109604

[8] Meng, Z., Shao, T., Liu, J., Li, J., Cao, L. and Fan, F. (2024) Scale-Demodulation Adaptive Chirp Mode Decomposition with Application to Rolling Bearing Fault Diagnosis. *IEEE Sensors Journal*, **24**, 32554-32565. https://doi.org/10.1109/jsen.2024.3443250

[9] Wang, W. (2021) Analysis of Fault Detection in Rolling Element Bearings. *IEEE Instrumentation & Measurement Magazine*, **24**, 42-49. https://doi.org/10.1109/mim.2021.9436098

[10] Kankar, P.K., Sharma, S.C. and Harsha, S.P. (2011) Fault Diagnosis of Ball Bearings Using Continuous Wavelet Transform. *Applied Soft Computing*, **11**, 2300-2312. https://doi.org/10.1016/j.asoc.2010.08.011

[11] Huang, N.E., Shen, Z., Long, S.R., Wu, M.C., Shih, H.H., Zheng, Q., *et al.* (1998) The Empirical Mode Decomposition and the Hilbert Spectrum for Nonlinear and Non-Stationary Time Series Analysis. *Proceedings of the Royal Society of London. Series A*: *Mathematical*, *Physical and Engineering Sciences*, **454**, 903-995. https://doi.org/10.1098/rspa.1998.0193

[12] Cheng, Y., Wang, Z. and Zhang, W. (2023) Combined Square Envelope Spectrum by Integrating Multiband Bearing Fault Information. *IEEE Sensors Journal*, **23**, 2495-2506. https://doi.org/10.1109/jsen.2022.3227244

[13] He, L., Li, X., Zhou, Q., Yi, C. and Li, Y. (2025) Neural Network Integrated with Classical Signal Processing Techniques for Generating Optimized Square Envelope Spectrum and Its Application in Machine Condition Monitoring. *IEEE Transactions on Instrumentation and Measurement*, **74**, Article ID: 3548311. https://doi.org/10.1109/tim.2025.3584118

[14] Wang, R., Xu, L. and Liu, F. (2020) Bearing Fault Diagnosis Based on Improved VMD and DCNN. *Journal of Vibroengineering*, **22**, 1055-1068. https://doi.org/10.21595/jve.2020.21187

[15] Li, C., Liu, Y. and Liao, Y. (2021) An Improved Parameter-Adaptive Variational Mode Decomposition Method and Its Application in Fault Diagnosis of Rolling Bearings. *Shock and Vibration*, **2021**, Article ID: 2968488. https://doi.org/10.1155/2021/2968488

[16] Xiao, C., Yang, P., Yue, S., Zhou, R. and Yu, J. (2024) Bearing Compound Fault Diagnosis Using Energy-Constrained Swarm Decomposition and Adaptive Spectral Amplitude Modulation. *IEEE Sensors Journal*, **24**, 18172-18184. https://doi.org/10.1109/jsen.2024.3392427

[17] Peng, D., Liu, Z., Jin, Y. and Qin, Y. (2019) Improved EMD with a Soft Sifting Stopping Criterion and Its Application to Fault Diagnosis of Rotating Machinery. *Journal of Mechanical Engineering*, **55**, 122-132. https://doi.org/10.3901/jme.2019.10.122

[18] Wang, L., Liu, Z., Miao, Q. and Zhang, X. (2018) Complete Ensemble Local Mean Decomposition with Adaptive Noise and Its Application to Fault Diagnosis for Rolling Bearings. *Mechanical Systems and Signal Processing*, **106**, 24-39. https://doi.org/10.1016/j.ymssp.2017.12.031

[19] Borghesani, P., Pennacchi, P., Randall, R.B., Sawalhi, N. and Ricci, R. (2013) Application of Cepstrum Pre-Whitening for the Diagnosis of Bearing Faults under Variable Speed Conditions. *Mechanical Systems and Signal Processing*, **36**, 370-384. https://doi.org/10.1016/j.ymssp.2012.11.001

[20] Chen, S., Yang, Y., Peng, Z., Wang, S., Zhang, W. and Chen, X. (2019) Detection of Rub-Impact Fault for Rotor-Stator Systems: A Novel Method Based on Adaptive Chirp Mode Decomposition. *Journal of Sound and Vibration*, **440**, 83-99. https://doi.org/10.1016/j.jsv.2018.10.010

[21] Wang, R., Han, W., Yu, L., Wang, C. and Hu, X. (2025) Adaptive Chirp Mode Decomposition Holo Spectral Analysis for Rolling Bearings Fault Diagnosis. *IEEE Sensors Journal*, **25**, 10707-10718. https://doi.org/10.1109/jsen.2025.3539423

[22] Wu, Q., Gao, Q., Lu, Y., Zhu, D., Sun, D., Zhao, D., *et al.* (2024) Incipient Fault Diagnosis Method via Joint Adaptive Signal Decomposition. *IEEE Sensors Journal*, **24**, 24308-24318. https://doi.org/10.1109/jsen.2024.3414299

[23] Ding, A., Tang, G., Wang, X., He, Y. and Fan, S. (2022) An Iterative Modified Adaptive Chirp Mode Decomposition Method and Its Application on Fault Diagnosis of Wind Turbine Bearings. *Machines*, **10**, Article No. 704. https://doi.org/10.3390/machines10080704

[24] Shi, G., Qin, C., Xia, P., Zhang, Z. and Liu, C. (2026) Generalized Envelope Nonlinear Gini Index-Gram Guided Two-Stage Chirp Mode Decomposition for Shield Machine Main Bearing Fault Diagnosis. *Advanced Engineering Informatics*, **71**, Article ID: 104354. https://doi.org/10.1016/j.aei.2026.104354

[25] Yao, X., Lv, Y., Yang, X., Wang, F. and Zheng, Y. (2024) An Adaptive Chirp Mode Decomposition-Based Method for Modal Identification of Time-Varying Structures. *Mathematics*, **12**, Article No. 3157. https://doi.org/10.3390/math12193157

[26] Leite, V.C.M.N., Silva, J.G.B.d., Torres, G.L., Veloso, G.F.C., Silva, L.E.B.d., Bonaldi, E.L., *et al.* (2017) Bearing Fault Detection in Induction Machine Using Squared Envelope Analysis of Stator Current. In: *Bearing Technology*, InTech, page. https://doi.org/10.5772/67145

[27] Antoni, J. (2016) The Infogram: Entropic Evidence of the Signature of Repetitive Transients. *Mechanical Systems and Signal Processing*, **74**, 73-94. https://doi.org/10.1016/j.ymssp.2015.04.034